A first principles calculation of the KLV Auger profiles of simple metals

1991 J. Phys.: Condens. Matter 3 641

(http://iopscience.iop.org/0953-8984/3/6/002)

J. Phys.: Condens. Matter 3 (1991) 641–653. Printed in the UK

A first principles calculation of the KLV Auger profiles of simple metals

P S Fowles†, J E Inglesfield‡ and P Weightman†

† Department of Physics and Surface Science Research Centre, University of Liverpool, Liverpool L69 3BX, UK

‡ Department of Physics, Catholic University of Nijmegen, Toernooiveld, 6525 ED Nijmegen, Netherlands

Received 16 July 1990

Abstract. We model the local electronic structure around a core-ionized site in a simple metal self-consistently using an embedding technique. We consider the local densities of states of Na, Mg and Al and calculate from first principles KLV Auger profiles. The success of this approach is assessed by comparison with experiment and with approximations which may be used to simplify the calculation. The agreement with experiment is on the whole good although some discrepancy arises for the case of $KL_{2,3}V$ lineshapes.

1. Introduction

Auger spectroscopy can yield valuable information on the local electronic structure of metals [1–3]. In simple metals it has been used to determine the orbital character of the local valence charge in the ground state and of the screening charge around core-ionized sites, it has been used to check the accuracy of calculations of the local density of states in the ground state and core-ionized states and to show up changes in these local densities of states brought about by alloying with other simple metals and with d band metals [1, 2, 4].

As a result of several recent studies [4–13] it is well established that for simple metals with wide bands of s and p valence character, Auger spectroscopy obeys the final state rule [5, 7, 14, 15]. Consequently, in the case of core–core-valence (CCV) transitions it should be possible to use the Auger profile to gain an insight into the nature of the distortion of the local density of states (DOS) produced by the final state core hole. Unfortunately, it is not completely clear how this information can best be extracted from the experimental Auger lineshape. A central question is now closely the spectral profiles of CCV transitions reflect the local DOS in the final core-ionized state and how much they are influenced by matrix element effects. If the energy dependence of the Auger matrix elements is small enough it is useful to decouple these into contributions from transition rates for final states of particular orbital character and contributions from the local DOS. This approximation yields an expression of the form,

$$A_{CCV}(E) = |M_{CCV_s}|^2 D_s(E) + |M_{CCV_p}|^2 D_p(E) \tag{1}$$

0953-8984/91/060641 + 13 $03.50

where M_{CCVl} is an energy-independent matrix element involving a final state of orbital character l and $D_l(E)$ is the corresponding angular decoupled density of states. This approximation is often made [4, 11, 13] since it provides a considerable simplification when constructing a model for the Auger profile.

In this paper we determine the local DOS, self-consistently, for core-ionized Na, Mg and Al, using a simple embedding [16] scheme, and calculate the KLV Auger profiles of these metals from first principles starting from Fermi's golden rule. Using these calculations and comparison with experimental data we assess the relative importance of the different contributions to the Auger profile and in particular the validity of the approximations leading to (1). We also study the spatial dependence of the Auger matrix elements, which enables us to determine the extent of the local electronic structure of simple metals probed by CCV Auger processes.

2. Experimental details

The magnesium KL_1V and $KL_{2,3}V$ Auger spectra were excited by AlK_α x-rays and measured using a modified AEI ES200 electron spectrometer fitted with a nine channeltron multidetector [17]. The experiments were performed in a vacuum of $<10^{-9}$ Torr and the sample was mechanically scraped every 2.5 hours so that contamination levels of oxygen and carbon, determined from photoelectron cross sections [18] and escape depths [19], amounted to <0.1 and <0.2 monolayers respectively. The KLV spectra of pure Mg has been measured many times and the results of our experiments (figure 1) are in good agreement with those of previous studies [8, 11, 12, 20]. Figure 1 shows the region of the electron spectrum of Mg to high kinetic energy of the KLL spectra. The first feature is the well known [21, 22] plasmon gain peak which accompanies the intense $KL_{2,3}L_{2,3}:{}^1D_2$ component which occurs at a lower energy than the spectral region shown in the figure. In order of increasing kinetic energy the spectrum next shows two photoelectron peaks: the C 1s peak arising from residual contamination and the Mg 2p internal photoemission peak excited by fluorescence x-rays from the Mg specimen. The next feature is the double peaked KL_1V Auger transition which is the principal interest of

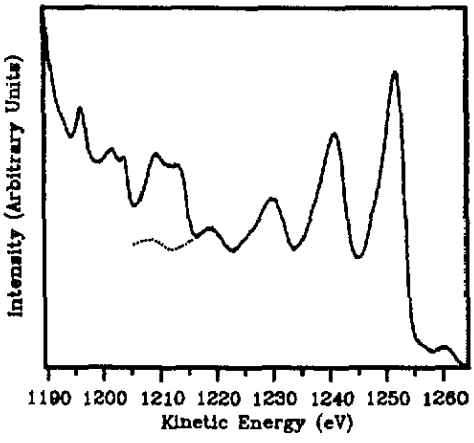

Figure 1. The region of the Mg photoelectron spectrum containing the KLV Auger transitions.

this study. To higher kinetic energy are three plasmon loss lines which accompany the intense $KL_{2,3}V$ Auger feature. The spectral profile of the $KL_{2,3}V$ transition also has two components but the low kinetic energy component is much weaker than that in the KL_1V profile and can only be discerned as a shoulder on the low kinetic energy side of the spectral profile.

The Mg KL_1V profile provides a suitable test of the model to be developed later since it displays a marked difference in shape from that of the valence band measured using photoemission. Since it is our intention to calculate the Auger profile of the KL_1V transition it is clearly important to allow for the influence on the measured shape of the KL_1V spectrum of the fourth and fifth plasmon losses accompanying the higher energy $KL_{2,3}V$ transition. Fortunately we are able to deduce the contribution from these processes by scaling and matching the appropriate spectral region of the first and second plasmons with the third plasmon and continuing the spectrum under the KL_1V profile. This continuation of the plasmon spectrum is shown by the dots in figure 1. It will later be added to the calculated spectral profile of the KL_1V transition when this is compared with experiment. The spectrum of the KL_1V transition also includes a background of scattered electrons which it is difficult to estimate but the intensity of which is expected to vary smoothly with energy. The measured KLV profiles also include contributions from instrumental and lifetime broadening processes. The instrumental broadening [23] contribution is well represented by a Gaussian of 0.5 eV full width at half maximum (FWHM) and the lifetime broadenings of the K and L shell core levels have been determined by XPS [23, 24].

3. Theoretical details

We treat the core-ionized atom as an impurity within the host material and relate the host and impurity using the embedding technique. Our approach neglects band structure effects, the host being considered to be free-electron-like with the correct Fermi energy and mean charge density for the system being considered. The valence wavefunctions in the impurity region are matched across the Wigner–Seitz radius onto the wavefunctions within the host. Matching is achieved implicitly, in the embedding method, by adding an embedding potential onto the Hamiltonian of the finite-sized impurity region, which may then be treated in isolation. The impurity potential itself is found self-consistently within the Wigner–Seitz radius from the impurity charge density by solving Poisson's equation for the electrostatic (Hartree) contribution and adding a local density exchange correlation term within the Hedin–Lundqvist approximation [25]. Rather than calculating the individual valence wavefunctions explicitly, we calculate the Green function, defined as:

$$G(\boldsymbol{r}, \boldsymbol{r}'; E) = \sum_i \frac{\psi_i(\boldsymbol{r})\psi_i^*(\boldsymbol{r}')}{E_i - E}. \tag{2}$$

This is expanded in terms of basis functions, $\chi(\boldsymbol{r})$, within the impurity region:

$$G(\boldsymbol{r}, \boldsymbol{r}'; E) = \sum_{i,j} G_{ij}(E)\chi_i(\boldsymbol{r})\chi_j^*(\boldsymbol{r}'). \tag{3}$$

We find it convenient to use as basis functions $u_{l;E}$ and $\dot{u}_{l;E'}$, at each l; $u_{l;E'}$ is the solution of the radial Schrödinger equation within the impurity atomic cell at a fixed energy E',

and $\dot{u}_{l,E'}$ is its energy derivative. These basis functions are entirely analogous to the functions entering the linear muffin tin orbital (LMTO) bandstructure method and are ideal for this localized impurity problem. From the Green function we are able to find the local DOS, defined as:

$$\sigma(r, E) = \sum_i \delta(E - E_i)|\Psi_i(r)|^2 \tag{4}$$

this is the charge density of states at a particular energy E. Comparing this result with (2) we see that:

$$\sigma(r, E) = (1/\pi)\,\mathrm{Im}\,G(r, r; E + i\varepsilon). \tag{5}$$

The charge density itself may be found by integrating $\sigma_i(r, E)$ over occupied states, and then we proceed to self-consistency.

Once the Green function is known we proceed by calculating the Auger line shape from first principles, starting from Fermi's golden rule:

$$P(E) = 2\pi \sum_{A,v} \frac{1}{2l_{c_i}+1}\delta(E + E_{c_i} - E_{c_f} - E_v) \sum_{m_{c_i}=-l_{c_i}}^{l_{c_i}} \sum_{m_{c_f}=-l_{c_f}}^{l_{c_f}} \langle M^2_{A;c_i;c_f;v}\rangle \tag{6}$$

where A, c_i, c_f, v represent the Auger, initial state core hole, final state core hole and valence electrons respectively. In the expression above, the matrix-element-square term may be written [26] as:

$$\langle M^2_{A;c_i;c_f;v}\rangle = 2[|D_{A;c_i;c_f;v}|^2 + |E_{A;c_i;c_f;v}|^2 - \mathrm{Re}(D_{A;c_i;c_f;v}E_{A;c_i;c_f;v})] \tag{7}$$

where the direct and exchange integrals are defined by:

$$D_{A;c_i;c_f;v} = \int dr_1\, dr_2\, \psi^*_{c_i}(r_1)\psi_{c_f}(r_1)\frac{e^2}{|r_1 - r_2|}\psi_v(r_2)\psi^*_A(r_2) \tag{8}$$

$$E_{A;c_i;c_f;v} = \int dr_1\, dr_2\, \psi^*_{c_i}(r_1)\psi_v(r_1)\frac{e^2}{|r_1 - r_2|}\psi_{c_f}(r_2)\psi^*_A(r_2). \tag{9}$$

Here we have averaged over the spins of the initial core hole and summed over other spins. Following Feibelman and McGuire [26] we separate D and E into radial and angular integrals:

$$D_{A;c_i;c_f;v}(E) = \sum_K \mathscr{D}_K(l_A, l_{c_i}, l_{c_f}, l_v; E)\mathscr{A}_{A;c_i;c_f;v}(K) \tag{10}$$

$$E_{A;c_i;c_f;v}(E) = \sum_K \mathscr{E}_K(l_A, l_{c_i}, l_{c_f}, l_v; E)\mathscr{A}_{A;c_i;c_f;v}(K) \tag{11}$$

where $\mathscr{A}$ is an angular integral and the radial matrix elements $\mathscr{D}$ and $\mathscr{E}$ are given by:

$$\mathscr{D}_K(l_A, l_{c_i}, l_{c_f}, l_v; E) = \int r_1^2\, dr_1 \int r_2^2\, dr_2 \psi_{c_i}(r_1)\psi_{c_f}(r_1)\frac{r_<^K}{r_>^{K+1}}\psi_A(r_2)\psi_v(r_2) \tag{12}$$

$$\mathscr{E}_K(l_A, l_{c_i}, l_{c_f}, l_v; E) = \int r_1^2\, dr_1 \int r_2^2\, dr_2\, \psi_{c_i}(r_1)\psi_v(r_1)\frac{r_<^K}{r_>^{K+1}}\psi_A(r_2)\psi_{c_f}(r_2). \tag{13}$$

Evaluating the angular integrals we obtain expressions for the KL_1V and $KL_{2,3}V$ transitions in terms of the radial matrix elements. Hence for KL_1V transitions, which

correspond to $l_{c_i} = l_{c_f} = 0$, we find

$$P(E) = 4\pi \sum_{A,l_A;v} \delta(E + E_{c_i} - E_{c_f} - E_v)\{(2l_A + 1)\mathfrak{D}_0^2(l_A, 0, 0, l_A; E) + \frac{1}{(2l_A + 1)}\mathfrak{C}_{l_A}^2(l_A, 0, 0, l_A; E) - \mathfrak{D}_0(l_A, 0, 0, l_A; E)\mathfrak{C}_{l_A}(l_A, 0, 0, l_A; E)\} \tag{14}$$

and for $KL_{2,3}V$ transitions, where $l_{c_i} = 0, l_{c_f} = 1$, then

$$P(E) = 4\pi \sum_{A,l_A;v,l_v} \delta(E + E_{c_i} - E_{c_f} - E_v) \int_{-1}^{1} dx\, P_1(x)P_{l_A}(x)P_{l_v}(x) \times \left\{\frac{(2l_A + 1)(2l_v + 1)}{6}\mathfrak{D}_1^2(l_A, 0, 1, l_v; E) + \frac{3}{2}\frac{2l_A + 1}{2l_v + 1}\mathfrak{C}_{l_v}^2(l_A, 0, 1, l_v; E) - \frac{2l_A + 1}{2}\mathfrak{D}_1(l_A, 0, 1, l_v; E)\mathfrak{C}_{l_v}(l_A, 0, 1, l_v; E)\right\}. \tag{15}$$

Consider a typical expression, for example, from equation (14)

$$\sum_v \delta(E + E_{c_i} - E_{c_f} - E_v)\mathfrak{D}_0^2(l_A, 0, 0, l_A; E) = \sum_v \delta(E + E_{c_i} - E_{c_f} - E_v) \times \int r_1^2\, dr_1\, r_2^2\, dr_2\, \psi_{c_i}\psi_{c_f}\frac{1}{r_>}\psi_A\psi_v \int r_3^2\, dr_3\, r_4^2\, dr_4\, \psi_{c_i}\psi_{c_f}\frac{1}{r_>}\psi_A\psi_v. \tag{16}$$

Then, using the expression for G_l, the lth angular momentum component from equation (2), this becomes

$$\sum_v \delta(E + E_{c_i} - E_{c_f} - E_v)\mathfrak{D}_0^2(l_A, 0, 0, l_A; E) = \frac{1}{\pi}\int r_1^2\, dr_1\, r_2^2\, dr_2\, r_3^2\, dr_3\, r_4^2\, dr_4\, \psi_{c_i}\psi_{c_f} \times \frac{1}{r_>}\psi_A\, \mathrm{Im}\, G_l(r_2, r_4; E + E_{c_i} - E_{c_f})\frac{1}{r_>}\psi_A\frac{1}{r_>}\psi_{c_i}\psi_{c_f} \tag{17}$$

where G_l is considered over the occupied valence levels up to the Fermi edge. Now we may write G_l in the separable form

$$\frac{1}{\pi}\mathrm{Im}\, G_l(r, r'; E) = \sum_{i,j} u_i(r)u_j(r')S_{i,j}^l(E) \tag{18}$$

where $i = 1, 2; j = 1, 2; u_1 = u, u_2 = \dot{u}$.

Equation (17) then becomes

$$\sum_v \delta(E + E_{c_i} - E_{c_f} - E_v)\mathfrak{D}_0^2(l_A, 0, 0, l_A; E) = \sum_{i,j} S_{i,j}^{l_A}(E) \times \int r_1^2\, dr_1\, r_2^2\, dr_2\, \psi_{c_i}\psi_{c_f}\frac{1}{r_>}\psi_A u_i \int r_1^2\, dr_1\, r_2^2\, dr_2\, \psi_{c_i}\psi_{c_f}\frac{1}{r_>}\psi_A u_j. \tag{19}$$

From this expression it may be seen that

$$\sum_{v} \delta(E + E_{c_i} - E_{c_f} - E_v)\mathfrak{D}_0^2(l_A, 0, 0, l_A; E)$$

$$= \sum_{i,j} S^{l_A}_{i,j}(E)\mathfrak{D}_{0;i}(l_A, 0, 0, l_A; E)\mathfrak{D}_{0;j}(l_A, 0, 0, l_A; E) \tag{20}$$

where the subscripts i and j denote that the valence wavefunctions ψ_v have been replaced in the expressions for the radial matrix elements, (equations (12) and (13)), by the basis functions u_i and u_j. Thus equations (14) and (15) may be written as

$$P(E) = 4\pi \sum_{l_A,i,j} S^{l_A}_{i,j}(E + E_{c_i} - E_{c_f}) \{(2l_A + 1)$$

$$\times \mathfrak{D}_{0;i}(l_A, 0, 0, l_A; E)\mathfrak{D}_{0;j}(l_A, 0, 0, l_A; E)$$

$$+ \frac{1}{(2l_A + 1)} \mathfrak{E}_{l_A;i}(l_A, 0, 0, l_A; E)\mathfrak{E}_{l_A;j}(l_A, 0, 0, l_A; E)$$

$$- \mathfrak{D}_{0;i}(l_A, 0, 0, l_A; E)\mathfrak{E}_{l_A;j}(l_A, 0, 0, l_A; E)\} \tag{21}$$

for KL_1V, and

$$P(E) = 4\pi \sum_{l_A,l_v,i,j} S^{l_v}_{i,j}(E + E_{c_i} - E_{c_f}) \int_{-1}^{+1} dx\, P_1(x)P_{l_A}(x)P_{l_v}(x)$$

$$\times \left\{ \frac{(2l_A + 1)(2l_v + 1)}{6} \mathfrak{D}_{1;i}(l_A, 0, 1, l_v; E)\mathfrak{D}_{1;j}(l_A, 0, 1, l_v; E) \right.$$

$$+ \frac{3(2l_A + 1)}{2(2l_v + 1)} \mathfrak{E}_{l_v;i}(l_A, 0, 1, l_v; E)\mathfrak{E}_{l_v;j}(l_A, 0, 1, l_v; E)$$

$$\left. - \frac{2l_A + 1}{2} \mathfrak{D}_{1;i}(l_A, 0, 1, l_v; E)\mathfrak{E}_{l_v;j}(l_A, 0, 1, l_v; E) \right\} \tag{22}$$

for $KL_{2,3}V$.

In addition to the Green function we need to know the core and Auger electron wavefunctions. The core wavefunctions are evaluated inside the muffin-tin using the Dirac equations with our self-consistent potential. The Auger electron energy is determined by the δ-function in (6), and at each energy the radial Schrödinger equation is integrated outwards numerically up to the Wigner–Seitz radius, where matching onto the free electron states determines the energy normalization [27].

The kinetic energy of the electrons emitted in the Auger process depends upon the binding energy of the core holes in the initial and final states. In our calculations these quantities were determined from the eigenvalues obtained for the appropriate orbitals, by solving the Dirac equations for the relaxed core-ionized final state, within our embedding scheme. By Koopman's theorem we equate these eigenvalues with the core-hole binding energies. Unfortunately the local density approximation is known to underestimate the binding energy of atomic core hole states [28] and the use of Koopman's theorem is also known to be inaccurate for deep holes due to relaxation effects [29]. Hence our calculations of the Auger electron kinetic energies do not agree with experiment. Our results for the ground state binding energies E_{1s}, E_{2s}, $E_{2p_{1/2}}$ and

$E_{2p_{3/2}}$ are 1248.7 eV, 75.1 eV, 42.7 eV and 42.2 eV respectively. These results underestimate the experimental values [30] by 54.3 eV, 13.5 eV and ~7 eV respectively. Our theoretical results for core binding energies give Auger energies of 1179.6 eV and 1212.8 eV for the Fermi edge of the KL_1V and $KL_{2,3}V$ transitions respectively. In order to compare our theoretical profiles with the experimental results we introduce shifts of 34.8 eV and 40.5 eV into our theoretical energy scale for the KL_1V and $KL_{2,3}V$ respectively in order to line up the two sets of spectra at the Fermi level.

The use of the embedding technique with our atomic basis functions, u_l and $\dot{u}_l$, offers two advantages. Firstly, the charge density is easily evaluated, requiring only an integration of the Green function. Thus by integrating $\sigma_l(r, E)$ over occupied states and up to the Wigner–Seitz radius we obtain local valence configurations in the ground state and around a core-ionized site in Mg of $3s^{1.0}3p^{1.0}$ and $3s^{1.4}3p^{1.6}$ respectively. Secondly, it is easy to study the consequences of simplifying the expression for the Auger transition in a manner similar to (1). If the energy of the Auger electron is assumed to be a constant lying within the allowed energy range then the expression becomes considerably less complex since radial and energy dependent parts separate, reducing by a large factor the time required for the calculation. Providing the Auger electron wavefunction does not vary greatly through the band this approximation should yield results in good agreement with those of the full calculation. This approach is more rigorous than (1) since the only approximation is that the Auger wavefunction is kept constant whereas (1) assumes that the matrix element is independent of the variation with energy of both the valence and Auger wavefunctions. As the range over which the Auger electron energy may vary is strictly limited, the transition rate information obtained from this calculation should give a good approximation to the full calculation. In section 4 we assess the usefulness of this simplified approach.

In principle it is necessary to evaluate the integrals in (12) and (13) over all space. Of course the localized core states limit the range of integration in the exchange term, but in the direct term there is no obvious cut off. However it is completely satisfactory to integrate only up to the Wigner–Seitz radius, since we find that truncating the integral at this radius introduces negligible errors.

4. Results and discussion

In comparing the calculated and experimental Auger profiles we begin with the angular decomposed local DOS within the neutral Wigner–Seitz sphere for the ground state (figure 2(*a*)) and for a core-ionized site (figure 2(*b*)). It can be clearly seen that the core-hole distorts the shape of the local s DOS, shown by the dashed curve, but leaves the shape of the local p DOS, shown by the dot–dashed curve, unchanged. This behaviour is in accordance with the results of previous studies [5–13]. Figure 2(*c*) and 2(*d*) show the calculated KL_1V and $KL_{2,3}V$ profiles respectively obtained from evaluating equations (21) and (22). A comparison of figure 2(*b*) and 2(*c*) shows the extent to which the contributions of the local s and p DOS to the Auger profile are modified by matrix element effects. As this comparison shows, the calculated KL_1V Auger profile (full curve figure 2(*c*)) is very similar to the shape of the total DOS around a core-ionized site (full curve figure 2(*b*)). However the matrix elements radically change the energy dependence of the relative contributions of the local s and p DOSS to the Auger profile from that expected on the basis of the local DOS alone. Figure 2(*e*) illustrates the KL_1V profile calculated

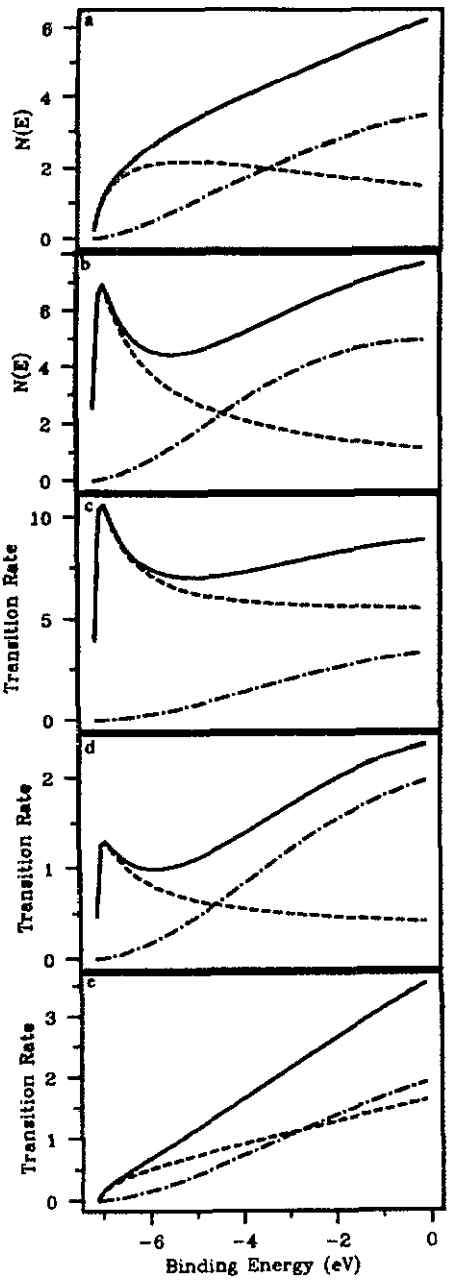

Figure 2. The calculated profiles of Mg for (*a*) the local DOS of the ground state, (*b*) the local DOS of a core-ionized site, (c) the KL_1V Auger transition, (d) the $KL_{2,3}V$ Auger transition and (*e*) the KL_1V Auger transition calculated using wavefunctions obtained from the ground state potential. In each figure the full curve shows either the total DOS or the total Auger profile while the contributions from s and p valence states are shown by the dashed and chain curves respectively. In these figures the local DOS are expressed in au while the transition rates for KL_1V and $KL_{2,3}V$ transitions are expressed in 10^{-4} au and 10^{-3} au respectively.

using wavefunctions derived from the potential for the ground state configuration. The influence of the core hole on the KL_1V Auger profile can be clearly seen by a comparison of figures 2(*c*) and 2(*e*).

In order to compare with experiment we convolute the calculated KL_1V profile (figure 2(*c*)) with the instrumental contribution and with a Lorentzian of FWHM 0.81 eV to represent the lifetime broadening contribution from the core levels [23, 24]. We also

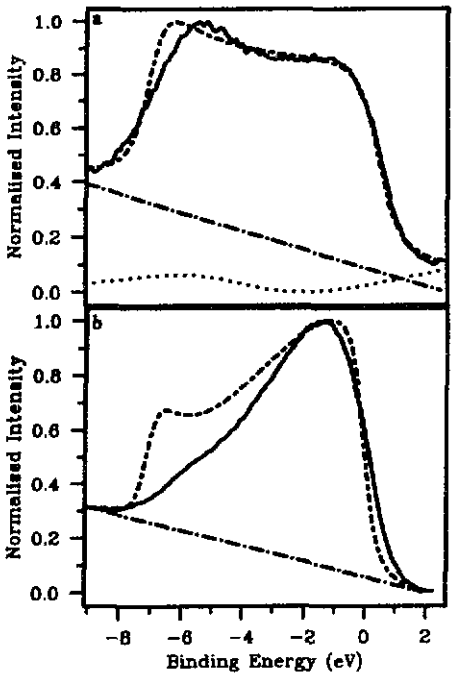

Figure 3. The full curves are the experimental profiles for Mg KL_1V (*a*) and $KL_{2,3}V$ (*b*) Auger transitions. The dashed curves are the theoretical profiles obtained by convoluting the results shown in figure 2 with lifetime and experimental broadening contributions as described in the text. The linear backgrounds and, in (*a*) the plasmon contributions are shown by the lower curves.

add the plasmon loss contribution discussed earlier and a smooth linear background. The two background contributions are shown separately by the lower curves in figure 3(*a*). This yields the dashed curve in figure 3(*a*) which may be compared with the experimental spectrum shown in the same figure. The equivalent comparison between the experimental and theoretical $KL_{2,3}V$ profile is shown in figure 3(*b*) where the lifetime broadening contributed by the core holes is a Lorentzian of FWHM 0.38 eV [23, 24]. Of course the underlying contributions of the valence s and p DOS to the calculated KL_1V and $KL_{2,3}V$ profiles are identical, the difference between the two is caused by matrix element effects. The calculated profile is in very good agreement with experiment for the KL_1V transition though it slightly overestimates the sharpness of the contribution from the s local DOS at high binding energy. The discrepancy between theory and experiment at the bottom of the band is more serious for the $KL_{2,3}V$ transition where the calculation appears to overestimate both the sharpness and the intensity of the contribution from the s local DOS. The high binding energy region of both spectra is susceptible to inaccuracy in the assumed form of the background contribution from energy loss processes and it is possible that the small discrepancy in the KL_1V case can be attributed to this. However, it seems unlikely that the uncertainty in the background contributions could explain all the discrepancy for the $KL_{2,3}V$ case where the broadening of the experimental spectrum appears to be greater than would be expected from the 0.38 eV contributions of the K and $L_{2,3}$ linewidths alone.

It is unlikely that the discrepancy between theory and experiment at the bottom of the band arises from our neglect of band structure effects since this might be expected to have a comparable effect on the spectral profiles of both transitions. It is possible that the discrepancy might be removed by a more accurate treatment of the wavefunction of the outgoing Auger electron since this could result in a shift in the balance of s and p

contributions to the spectra. An alternative possibility is that the discrepancy arises from the lifetime broadening of the single particle states within the valence band. These may decay by Auger and other processes and the deeper the hole state in the valence band the shorter will be its lifetime so that there will be greater broadening at the bottom of the band where the discrepancy lies. Lansberg's calculations [31] indicate that such broadening is of the order of 1 eV and lifetime broadening of this order has also been observed for localized valence holes in a number of d band metals and alloys (see [32] and references therein). A lifetime broadening of about 1 eV would be enough to remove the discrepency between theory and experiment for the $KL_{2,3}V$ profile. Of course such final state lifetime broadening will also contribute to the KL_1V profile though it may be that the need to invoke such a contribution is hidden in this spectrum by the larger lifetime broadening (0.81 eV) contributed by the core levels.

We may make one further comparison with experiment by considering the intensity ratio of the $KL_{2,3}V$:KL_1V maxima. We obtain a value of 2.7 for the relative intensity of the $KL_{2,3}V$:KL_1V maxima from the calculation, which is in quite good agreement with the value of 4.0 ± 1.0 obtained from experiment after an estimate of the background contribution.

4.1. Application to Na and Al

In order to further test our model and to allow comparison with previous work we performed similar calculations for two other simple metals, Na and Al, experimental KLV spectra for both of which have been published previously [33, 34]. Our results for the KL_1V and $KL_{2,3}V$ of Na and Al show similar degrees of agreement with experiment to that obtained for Mg.

4.2. Simplified analysis

We now consider the consequences of approximating the full expression for the Auger spectrum given in equation (21) by fixing the energy of the Auger electron instead of allowing this to vary through the valence band. This gives an expression similar to (1) but which retains the energy dependence of the valence wavefunctions. This simplified expression was evaluated using several values for the Auger energy within the energy range permitted by the δ-function in (6). The results obtained by calculating the Mg KL_1V lineshape in this way are shown in figure 4 where the full curve is the profile obtained using a constant Auger energy appropriate to a final state 0.3 eV below the Fermi energy. The transition rate decreases smoothly as the fixed Auger energy is reduced and the other curves in figure 4 correspond to final states at 1.7 eV, 3.0 eV, 4.4 eV, 5.7 eV and 7.1 eV below the Fermi energy.

A comparison of these results with the full calculation (figure 2(*c*)) shows that the agreement obtained is dependent on the choice of the Auger electron energy E_A However, apart from a tendency to overestimate the sharpness of the peak derived from the s DOS, the shape of the Auger profile given by the approximate treatment is similar to that of the complete first principles calculation. Choosing an Auger electron energy in the middle of the range yields a total transition rate that is in error from the full calculation by only 7%.

Our results confirm that both the local DOS and the Auger profile are influenced in a similar manner by the screening of the core hole by the valence electrons, though it is not clear that the two effects may be simply linked via equation (1). This can be seen from the following test of (1). We begin with the local DOS given by the embedding

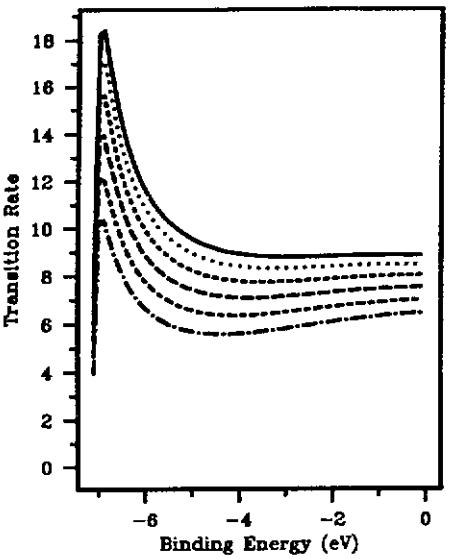

Figure 4. The Mg KL_1V Auger profiles obtained by fixing the Auger energy. The top curve corresponds to a final state at an energy of 0.3 eV below the Fermi energy. Lower curves correspond to final states with energies 1.7 eV, 3.0 eV, 4.4 eV, 5.7 eV and 7.1 eV below the Fermi energy respectively. The transition rates are expressed in 10^{-4} au.

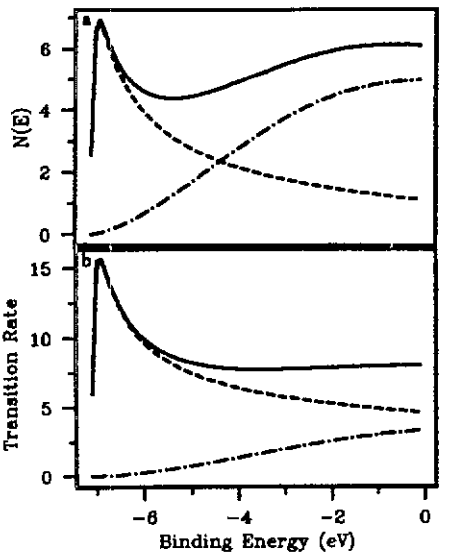

Figure 5. The best approximation to the Mg KL_1V profile (*a*) obtained from modifing the local s- and p-DOS using R_{cut} and $M_{KL_1V_s}/M_{KL_1V_p}$ as free parameters via equation (1). The Mg KL_1V profile (*b*), obtained by fixing the Auger electron energy in the centre of the band. The full curves show the overall profiles while the dashed and chain contributions show the individual s- and p-components. The transition rates are expressed in 10^{-4} au.

approach treating the radius over which the integration is performed to determine the local DOS, R_{cut}, as a free parameter. Combining this with the ratio $M_{KL_1V_s}/M_{KL_1V_p}$ as a second free parameter we can obtain a reasonable fit to the data as far as the overall shape is concerned but this approach gives a false indication of the individual contributions made by the s and p DOS to the overall lineshape, figure 5(*a*) (compare with figure 2(*c*)). The error arises from the assumption made in deriving (1) that the Auger matrix elements are independent of the energy of the valence wavefunctions. This can be seen from figure 5(*b*) where the Auger matrix elements have been calculated in the constant Auger energy approximation. The importance of including the energy dependence of the valence wavefunctions in the calculation can be seen from figure 6 which shows that the quantities $|M(KL_1V_s)|^2$ and $|M(KL_1V_p)|^2$ depend quite strongly on the valence energy and that even the ratio $|M(KL_1V_s)|^2/|M(KL_1V_p)|^2$ is too dependent on the valence energy for (1) to provide an accurate representation of the situation. Equation (1) neglects the changes with energy in both the valence and Auger electron wavefunctions, whereas the constant energy Auger electron approximation allows the valence wavefunctions to vary with energy. As we see by comparing figure 5(*b*) with the full calculation of figure 2(*c*), the constant Auger energy approximation describes the behaviour of the individual s and p contributions reasonably well, while preserving the computational simplicity of (1).

We now use the constant Auger energy approximation to assess the importance of

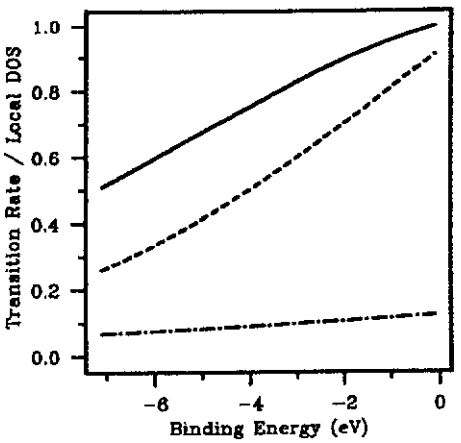

Figure 6. The dot–dashed line is the transition rate to p valence states divided by the p DOS, the dashed line is the transition rate to s valence states divided by the s DOS and the full line is the ratio of these two quantities.

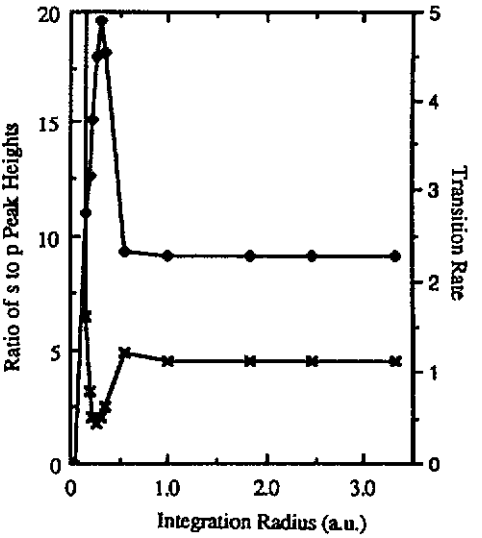

Figure 7. The dots show the dependence of the ratio of the peak heights of the s and p contributions to the calculated Mg KL_1V profile on the radius of integration. The crosses show the variation of the total transition rate for these processes on the radius of integration.

the cut-off radius to which the integrals in (12) and (13) are evaluated. Figure 7 shows the total transition rate and the ratio of the peak heights of the s and p local DOS contributions as a function of the radius of integration R_{cut}. As can be seen, increasing the integration cut-off beyond 1 au does not change either the size or the shape of the Auger profile. This is a consequence firstly of the localized core wavefunctions, which do not extend beyond ~0.5 au and cut off the exchange integral, and secondly of the very rapid oscillations in the Auger wavefunction which give rise to cancellation in the direct integral outside a range of 1 au.

4.3. Inadequacy of a square well treatment

In an earlier study [35] of the KL_1V spectrum of magnesium the core-ionized site was modelled by a simple square well potential within a free electron gas, and local s- and p-DOS were used to calculate the Auger profile via the approximation of equation (1). The ratio of the matrix elements, $M_{KL_1V_s}/M_{KL_1V_p}$ and R_{cut}, were used as free parameters to obtain a fit to experiment. This model yields a profile that compares well with the experimental spectra, but the square well required to give s- and p-DOS in agreement with the Auger profile is strong enough to pull off a bound state and this latter consequence was neglected in the analysis. In subsequent investigations we have determined that if the depth of the square well is reduced so that a bound state is no longer formed the simple model cannot reproduce the experimental profile. We conclude that the square well approach is inadequate for the description of the local electronic structure probed by CCV transitions in simple metals.

5. Conclusions

We have calculated the Auger profiles of CCV processes for Na, Mg and Al from first principles using a new and relatively simple treatment of the impurity problem in which the local DOS is determined self-consistently from an embedding scheme. Detailed comparisons with experimental results for Mg show that the theory, which neglects band structure effects, gives good agreement for the KL_1V transition but overestimate the sharpness and intensity of the contribution of the s DOS to the $KL_{2,3}V$ profile.

An approximate treatment which allows for the variation of the matrix elements with the energy of the valence electrons but neglects their dependence on the energy of the Auger electron gives quite a good representation of the overall CCV Auger profile and its dependence on the local s- and p-DOS.

References

[1] Cubiotti G, Mondio G and Wandelt K (ed) 1989 *Auger Spectroscopy and Electronic Structure* (Berlin: Springer)
[2] Thomson M, Baker M D, Christie A and Tyson J F (ed) 1985 *Auger Electron Spectroscopy* (New York: Wiley)
[3] Briant C L and Messmer R P (ed) 1989 *Auger Electron Spectroscopy* (New York: Academic)
[4] Weightman P 1989 *Phys. Scr.* **T25** 165
[5] von Barth U and Grossmann G 1983 *Phys. Scr.* **28** 107
[6] von Barth U and Grossmann G 1979 *Solid State Commun.* **32** 645
[7] von Barth U and Grossmann G 1980 *Phys. Scr.* **21** 580
[8] Lässer R and Fuggle J C 1982 *Phys. Rev.* B **25** 5150
[9] von Barth U and Grossmann G 1982 *Phys. Rev.* B **25** 5150
[10] Hannah P H, Weightman P and Andrews P T 1985 *Phys. Rev.* B **31** 6238
[11] Davies M, Weightman P and Jennison D R 1984 *Phys. Rev.* B **29** 5318
[12] Davies M and Weightman P 1984 *Phys. Rev.* B **30** 4183; 1985 *Phys. Rev.* B **32** 8423(E)
[13] Weightman P 1989 *Auger Spectroscopy and Electronic Structure* ed G Cubiotti, G Mondio and K Wandelt (Berlin: Springer)
[14] Jennison D R, Madden H H and Zehner D M 1980 *Phys. Rev.* B **21** 430
[15] Ramaker D E 1982 *Phys. Rev.* B **25** 7341
[16] Inglesfield J E 1981 *J. Phys. C: Solid State Phys.* **14** 3795
[17] Weightman P and Andrews P T 1980 *J. Phys. C: Solid State Phys.* **13** 3529
[18] Schofield J H 1976 *J. Electron Spectrosc.* **9** 29
[19] Penn D R 1976 *J. Electron Spectrosc.* **8** 129
[20] van Attekum P M Th M and Trooster J M 1979 *Phys. Rev.* B **20** 2335
[21] Abo-Namous S A, Andrews P T and Johnson C E 1979 *J. Phys. F: Metal Phys.* **9** 61
[22] Fuggle J C, Lässer R, Gunnarsson O and Schönhammer K 1980 *Phys. Rev. Lett.* **44** 1090
[23] Davies M, Hannah P H, Weightman P and Andrews P T 1984 *J. Phys. F: Metal Phys.* **14** 355
[24] Citrin P H, Wertheim G K and Baer Y 1977 *Phys. Rev.* B **16** 4256
[25] Hedin L and Lundqvist B I 1971 *J. Phys. C: Solid State Phys.* **4** 2064
[26] Feibelman P J and McGuire E J 1977 *Phys. Rev.* B **15** 3006
[27] Landau L D and Lifshitz E M 1965 *Quantum Mechanics* (New York: Pergamon)
[28] Almbladh C O and Pedroza A C 1984 *Phys. Rev.* A **29** 2322
Lundqvist S and Marsh N H 1983 *The Theory of the Inhomogeneous Electron Gas* (New York: Plenum)
[29] Weightman P 1982 *Rep. Prog. Phys.* **45** 753
[30] Fuggle J C and Martensson N 1980 *J. Electron Spectrosc.* **21** 275
[31] Landsberg P T 1949 *Proc. Phys. Soc.* A **62** 806
[32] Weightman P, Wright H, Waddington S D, van der Marel D, Sawatzky G A, Diakun G P and Norman D 1987 *Phys. Rev.* B **36** 9098
[33] Barrie A and Street F J 1975 *J. Electron Spectrosc.* 7 1
[34] van Attekum P M Th M and Trooster J M 1978 *Phys. Rev.* B **18** 3872
[35] Weightman P, Davies M and Inglesfield J E 1986 *Phys. Rev.* B **34** 6843